Attributable human-induced changes in the likelihood and magnitude of the observed extreme precipitation during Hurricane Harvey

Mark D. Risser[1] * and Michael F. Wehner[2]

Mark D. Risser, mdrisser@lbl.gov

[1]Climate and Ecosystem Sciences Division, Lawrence Berkeley National Laboratory

[2]Computational Research Division, Lawrence Berkeley National Laboratory

[*]1 Cyclotron Road, Berkeley, CA 94720

This article has been accepted for publication and undergone full peer review but has not been through the copyediting, typesetting, pagination and proofreading process, which may lead to differences between this version and the Version of Record. Please cite this article as doi: 10.1002/2017GL075888

Record rainfall amounts were recorded during Hurricane Harvey in the Houston, Texas area, leading to widespread flooding. We analyze observed precipitation from the Global Historical Climatology Network with a covariate-based extreme value statistical analysis, accounting for both the external influence of global warming and the internal influence of ENSO. We find that human-induced climate change *likely* increased the chances of the observed precipitation accumulations during Hurricane Harvey in the most affected areas of Houston by a factor of at least 3.5. Further, precipitation accumulations in these areas were *likely* increased by at least 18.8% (best estimate of 37.7%), which is larger than the 6-7% associated with an attributable warming of 1°C in the Gulf of Mexico and Clausius-Clapeyron scaling. In a Granger causality sense, these statements provide lower bounds on the impact of climate change and motivate further attribution studies using dynamical climate models.

Keypoints:

- Observations show that climate change *likely* increased Hurricane Harvey's total rainfall by at least 19%.
- Climate change *likely* increased the chances of the observed rainfall by a factor of at least 3.5.
- Observations suggest that changes exceeded Clausius-Clapeyron scaling, motivating dynamical studies.

1. Introduction

Hurricane Harvey made landfall on the coast of Texas on August 26, 2017 as a category 4 storm. Rather than proceeding to track inland and dissipate, Harvey stalled with a portion of the storm system remaining over the warm waters of the Gulf of Mexico for another four days. While damages from high winds were significant, it was the unprecedented amount of rain that fell on the greater Houston area from August 25 through August 31 and the resultant inland flooding that caused this tropical storm to be one of the most damaging since Hurricane Katrina in 2005. In this paper, we analyze observed precipitation in the Houston area with a non-stationary Generalized Extreme Value (GEV) statistical model ([*Coles*, 2001]). Saturation specific humidity increases in a warmer atmosphere according to the Clausius-Clapeyron relationship by about 6-7% per degree local warming in the absence of dynamical changes. As a result of this physical property of air, extreme precipitation is expected to increase by at least this amount as the climate warms due to anthropogenic changes in the composition of the atmosphere ([*Allen and Ingram*, 2002]). As the source of the moisture during Hurricane Harvey is clearly from the Gulf of Mexico near the Texas coastline, ocean temperature in the region is a logical choice for a physical covariate in a statistical model of extreme precipitation. However, our purposes here are to find an attributable human influence, if any, to the precipitation during the storm. Sea surface temperatures (SSTs) at any given time, even at the global scale, are determined by a mix of human and natural factors, and it is important to separate these factors for an attribution study ([*National Academy of Sciences*, 2016]). The El Nino/Southern Oscillation (ENSO) is the largest natural influence on SST as well as a significant factor in

modulating Atlantic hurricane activity ([*Patricola et al.*, 2014]). While we could remove the effect of ENSO on SST to construct a mostly anthropogenic covariate ([*Compo and Sardeshmukh*, 2010]), we instead isolate the human and natural effects on extreme precipitation by using two time-dependent covariates, total atmospheric CO_2 concentration and Niño3.4, a commonly used ENSO index. There are important caveats to this choice. First, other natural factors apart from ENSO are not accounted for and are "hidden" co-varying effects. Second, saturation specific humidity scales with temperature rather than atmospheric composition. Also, while CO_2 radiative forcings scale with its natural logarithm ([*Ramaswamy et al.*, 2001]) and determine equilibrium surface temperatures, the relationship to transient surface temperatures further depends on the efficacy of ocean heat uptake ([*Winton et al.*, 2010]). Despite these caveats, atmospheric CO_2 concentration and Niño3.4 are well measured and provide a reasonable, if not complete way to separate the human and natural influences on extreme precipitation.

2. Data

The data used for our analysis are daily weather station measurements of total precipitation (in millimeters) obtained from the Global Historical Climatology Network (GHCN) over a latitude/longitude box centered on Houston, Texas (covering 26.5°N to 33°N and 91°W to 99°W) from January 1, 1950 through September 10, 2017. Data files and a variety of instructional documentation are available at `ftp://ftp.ncdc.noaa.gov/pub/data/ghcn/daily/`; the data files used were downloaded at approximately 13:00 PDT on September 21, 2017. Details on data quality control and a plot of all available GHCN stations in the latitude/longitude box are provided in the supporting information.

2.1. Estimation of the Hurricane Harvey rainfall totals

The bulk of the precipitation over the Houston, Texas region was received from August 25, 2017 to August 31, 2017. Although the GHCN data are updated regularly, not all of the stations in this region contain values for all seven days. Thus, to ensure that our estimate of the weekly total is appropriate, we only retain stations that have at least five non-missing daily values during this seven-day period. The remaining individual station measurements are plotted in the left panel of Figure 1, along with a geostatistical filled-in prediction map (using a stationary Gaussian process model and kriging) in the center panel. For comparison, we also show the weekly total downloaded from the NOAA's Advanced Hydrologic Prediction Service (AHPS) in the right panel (`https://water.weather.gov/precip/index.php`), which are quality-controlled, multiple source (radar and rain gauge) precipitation estimates. The general pattern and amount of total precipitation during this week is consistent between the gridded GHCN station and AHPS estimates.

We have divided the GHCN stations into two groups. A larger region defined by the red ellipse (comprising approximately 105,000 km^2) contains 247 stations of which only 43 contain the requisite 5 non-missing daily values. A smaller region of 83 stations ⸨ defined by the orange ellipse ⸩ (comprising approximately 33,000 km^2) is centered on the highest values during this week. Only 11 of these stations satisfy our quality control criterion. A map with all of the GHCN stations in Louisiana and Texas is shown in the supporting information. Table 1 summarizes these estimates of Texas precipitation, averaged over all

stations or grid cells inside each station group, during Hurricane Harvey. We interpret the range in values for each region as a crude estimate of the observational uncertainty.

2.2. Historical data

To place the precipitation totals from Hurricane Harvey in a climatological context, we extract the largest seven-day rainfall total (denoted hereafter as Rx7day) for each GHCN station during hurricane season (July to November) for 1950-2016 from the daily precipitation measurements and calculated a simple arithmetic average as in Table 1. Rx7day values were only recorded if a station had a minimum of 66.7% of daily precipitation measurements in the July-November time interval in a given year, and the recorded Rx7day value refers to a complete seven-day interval with no missing values. While it varies across the time series, on average there are about 25 stations satisfying this quality control condition in the smaller region and about 80 such stations in the larger region. It is possible (but not likely) that the seasonal maximum values in a particular year occurred from different storms across the stations. The annual time series for each region over 1950-2016 is shown in Figure 2(a).

It should be noted that the even the lowest estimates of the precipitation total during Hurricane Harvey (see Table 1: 700.2mm for the small region and 481.6mm for the large region) are significantly larger than the previous record for each group of stations over 1950-2016 (315.8mm for the small region and 300.3mm for the large region). The 2017 storm totals are intentionally left off of the observed time series in Figure 2(a) in order to more appropriately visualize the variability over 1950-2016. We provide some discussion

in Section 5 on how the magnitude of the precipitation accumulations during Hurricane Harvey impact our analysis.

3. Extreme Value Analysis

An extreme value analysis was conducted for each group of stations based on the Rx7day time series in Figure 2(a) for 1950-2016. We intentionally exclude the 2017 observed precipitation values from our statistical model in order to perform an "out of sample" analysis of Hurricane Harvey precipitation in the sense of an *a priori* prediction. While there are several different ways to characterize the extreme values of an atmospheric process (see, e.g., [*Coles*, 2001]), we use a block maxima approach and the generalized extreme value (GEV) family of distributions. The block maxima approach specifies a statistical model for $Z_t = \max\{Y_{t1}, \ldots, Y_{tn}\}$, where the $\{Y_{ti}, i = 1, \ldots, n\}$ are individual measurements (here, seven-daily precipitation totals) within "block" t (here, July to November of year t). Statistical theory says that the cumulative distribution function (CDF) of Z_t is a member of the GEV family

$$G_t(z) \equiv \mathbb{P}(Z_t \leq z) = \exp\left\{-\left[1 + \xi_t\left(\frac{z-\mu_t}{\sigma_t}\right)\right]^{-1/\xi_t}\right\}, \quad (1)$$

defined for $\{z : 1+\xi_t(z-\mu_t)/\sigma_t > 0\}$. The GEV family of distributions (1) is characterized by three parameters: the location parameter $\mu_t \in \mathcal{R}$ (which describes the center of the distribution), the scale parameter $\sigma_t > 0$ (which describes the spread of the distribution), and the shape parameter $\xi_t \in \mathcal{R}$. The shape parameter ξ_t determines the qualitative behavior of the distribution of maximum Rx7day rainfall: if $\xi_t < 0$, the distribution has a finite upper bound of $\mu_t - \sigma_t/\xi_t$; if $\xi_t > 0$, the distribution has no upper limit; if $\xi_t = 0$,

the distribution is again unbounded and the CDF (1) is interpreted as the limit $\xi_t \to 0$ ([*Coles*, 2001]).

As the notation in (1) suggests, we wish to allow the GEV parameters $\{\mu_t, \sigma_t, \xi_t\}$ to vary over a set of years $\{t = 1, \ldots, T\}$, so that we can characterize changes in the distribution of Rx7day over time. As outlined in Section 1, two covariates are used to describe the temporal variations in extreme precipitation: seasonally-averaged global CO_2 and annually-averaged Niño3.4 index. While other choices of suitable covariates are possible, these two were chosen as they provide a clear distinction between natural and human influences. Niño3.4 values are based on the ERSSTv5 monthly index from NOAA's National Center for Environmental Prediction (`http://www.cpc.ncep.noaa.gov/data/indices/`). The CO_2 measurements are a combined time series of data used as input for climate models (from the International Institute for Applied Systems Analysis or IIASA; see `https://tntcat.iiasa.ac.at/RcpDb`) and the record from the Mauna Loa Observatory (MLO). The IIASA values are based on actual observations for 1950-2005, hence we extend these from 2006-2017 using the MLO values. We must use this combined time series to take advantage of the 1950-2016 GHCN data, as the MLO CO_2 record only goes back to 1958. The Niño3.4 and CO_2 covariates are plotted in the supporting information.

As with mean regression (also known as ordinary least squares), we can specify linear relationships between these covariates and the GEV parameters to estimate the coefficients for each covariate. Using the CO_2 and Niño3.4 covariates to characterize changes over time in Rx7Day, we consider four different trend models for the GEV parameters:

1. Model M0, where all of the GEV parameters are constant over time:

$$\mu_t \equiv \mu, \quad \sigma_t \equiv \sigma, \quad \xi_t \equiv \xi$$

2. Model M1, where both the location and scale parameters depend linearly on only $\ln(CO_2)$:

$$\mu_t = \beta_0 + \beta_1 x_{1t}, \quad \log \sigma_t = \phi_0 + \phi_1 x_{1t}, \quad \xi_t \equiv \xi$$

3. Model M2, where the location parameter depends linearly on both $\ln(CO_2)$ and Niño3.4 and the log of the scale parameter depends linearly on $\ln(CO_2)$ only:

$$\mu_t = \beta_0 + \beta_1 x_{1t} + \beta_2 x_{2t}, \quad \log \sigma_t = \phi_0 + \phi_1 x_{1t}, \quad \xi_t \equiv \xi$$

4. Model M3, where the location and log of the scale parameters depend linearly on both $\ln(CO_2)$ and Niño3.4:

$$\mu_t = \beta_0 + \beta_1 x_{1t} + \beta_2 x_{2t}, \quad \log \sigma_t = \phi_0 + \phi_1 x_{1t} + \phi_2 x_{2t}, \quad \xi_t \equiv \xi$$

In the above, $x_{1t} = \ln(CO_2)$ in year t and x_{2t} = the Niño3.4 index value for year t. We only consider models in which the shape is constant over time because we believe the data do not provide enough information to estimate a time-varying shape parameter. Our reasoning for this choice follows from *Cooley et al.* [2007], who found that a constant shape parameter yielded better results compared to a statistical model that allowed the shape parameter to vary across the domain of interest (in their case, over a spatial domain). The Akiake Information Criterion (AIC) clearly selects model M2 as best for both regions (see the supporting information for more details), indicating that model M2 preserves the most information of the four models tested.

Maximum likelihood estimation is used to obtain best estimates of all statistical parameters in model M2 for both groups of stations via the `climextRemes` package for `R` ([*Paciorek*, 2016]), and the bootstrap is used to quantify uncertainty in these estimates (see the supporting information for more details). The best estimates and the bootstrap are also used to estimate return values (i.e., quantiles of the distribution of Rx7day), return probabilities (i.e., the probability of a particular magnitude storm occurring in each year), and return periods (i.e., the inverse return probability); again see the supporting information. Note that this nonstationary model allows us to characterize changes over time by suitable variation of either or both of the two physical covariates, so that we can isolate the effects of both natural and human sources of variation in extreme precipitation.

4. Results

Best estimates and confidence intervals for each of the GEV coefficients for both regions are given the supporting information. The 90% confidence intervals of the CO_2 and Niño3.4 coefficients in the location parameters (β_1 and β_2) do not include zero, indicating that it is *very likely* that both human and natural processes cause observed changes over time in the center of the GEV distribution. In this statement as well as elsewhere in the paper, we use the terms *likely* and *very likely* as a confidence statement as defined by the Intergovernmental Panel on Climate Change (IPCC; [*Mastrandrea et al.*, 2010]). Although the best estimate of the CO_2 coefficient for the log scale parameter (ϕ_1) is positive, indicating that the variability of the GEV distribution increases with CO_2, the 66% confidence interval includes zero precluding an IPCC-style confidence statement about the anthropogenic influence on the variability of hurricane season maximum precipitation in

Texas. Finally, the best estimate of the shape parameter is positive ($\widehat{\xi} = 0.11$), meaning that the fitted distribution of Rx7day is heavy-tailed and unbounded (this is consistent with other extreme value analyses involving precipitation), but confidence intervals also include negative values, indicating the possibility of a bounded distribution. While the actual distribution of extreme precipitation is of course bounded, fitted unbounded distributions to extreme precipitation are not uncommon ([*Cooley et al.*, 2007]).

While estimates of the GEV coefficients can be insightful, for attribution purposes we are more interested in exploring how return values, return periods, and return probabilities have changed as a result of the anthropogenic increases in atmospheric CO_2 concentrations while accounting for the natural influence of ENSO. Conditional on the fitted statistical models, we first estimate the return periods in each region for the largest previously observed value of Rx7day, namely 315.8mm for the small region of Figure 1 and 300.3mm for the large region (these values both occurred in 1998; see Figure 2a). The best estimate of the return periods for these seven-day precipitation totals are shown from 1950 to 2017 in Figure 2(b) with a solid line. The 66% and 90% confidence intervals are shown with the dark and light bands, respectively. Note that the return period and confidence intervals are calculated for each year using observed values of both Niño3.4 and CO_2. The uncertainty is quite large at the 90% confidence level, but there is a steady decrease in the return periods for each region. This indicates that the largest previously observed Rx7day total has become much more commonplace: from a several hundred year storm in 1950 to a 25-50 year storm in 2017. Our covariate-based analysis indicates that this change is due to the anthropogenic increase in atmospheric CO_2 concentrations and not

natural ENSO variability. Figure 2(c) shows the change in return periods estimated using the station averages of Rx7day from Table 1 during Hurricane Harvey. Estimated return periods and their statistical uncertainties are significantly larger than for the previously largest observed precipitation total in Figure 2(a). A visual inspection of the return period plots in both Figure 2(b) and (c) reveals that large magnitude storms are becoming more common.

The covariate-based statistical models permit isolation of the effect of anthropogenic warming on the probability of large storms under fixed ENSO conditions. This is accomplished by first estimating the probability of the Rx7day total in the current year, Z^*, exceeding some threshold z conditional on a fixed Niño3.4 index, say that observed in 2017, and on CO_2 concentrations in that same year, or

$$p_1(z) \equiv \mathbb{P}(Z^* > z \,|\, \text{2017 values of Niño3.4 and } CO_2)$$

(the vertical bar "|" means "conditional on"). Next, we calculate a similar probability, but in a counterfactual world with a similar ocean state (as described by the Niño3.4 index) but earlier (say 1950) CO_2 concentrations,

$$p_0(z) \equiv \mathbb{P}(Z^* > z \,|\, \text{2017 Niño3.4 but 1950 levels of } CO_2).$$

Comparison of the likelihood of events of fixed magnitude is commonly termed "probabilistic event attribution" ([*Pall et al.*, 2014]), and explores the ratio of these probabilities referred to as the "risk ratio" for z,

$$RR(z) = \frac{p_1(z)}{p_0(z)} \tag{2}$$

(see, e.g., [*Jeon et al.*, 2016]; [*Risser et al.*, 2017]; [*Paciorek et al.*, 2017]). Here, we mean "risk" in the epidemiological or relative sense. Figure 2(d) shows the best estimate of this risk ratio in each region for precipitation totals ranging from 300mm to 1000mm (solid line) as well as a *likely* (66%) lower confidence bound. The best estimate of the risk ratio in both regions is larger than 4 over this entire range of precipitation totals. The *likely* lower bound on the risk ratio is decidedly larger than 1 for both regions and all values of z, and in fact is larger than 3 for the small region. For the average station data totals (see Table 1: 735.0mm for the small region and 491.6mm for the large region), the best estimate of the risk ratio is 9.6 (with a *likely* lower bound of 3.5) in the small region and 5.0 (with a *likely* lower bound of 1.4) in the large region. These risk ratio lower bound estimates are notably insensitive to choice of the value of z, and hence would not change much across the observational uncertainty of the Hurricane Harvey precipitation totals (Table 1) or even much larger storm total uncertainty estimates.

It is important note that our analysis is based only on observational data. Therefore, any attribution statement made here must be interpreted in the Granger causality sense ([*Granger*, 1969]) as a measure of predictability based on the statistical model. The more traditional framework for event attribution studies ([*National Academy of Sciences*, 2016]) uses Pearl's definition of causality ([*Pearl*, 1988; *Hannart et al.*, 2016]), which is based on intervention (e.g., using dynamical climate models to construct a counterfactual climate scenario) and can be used to prove causal connections. Observational analyses with Granger causality cannot prove causal connections, but are still powerful in that they can disprove causal connections as well as establish a lower bound for an attribution

statement like the risk ratio ([*Ebert-Uphoff and Deng*, 2012]). For Hurricane Harvey, our predictive model suggests that there is a *likely* human induced increase in the chances of reaching the observed rainfall totals since the risk ratio is well above one for both regions considered and over a wide range of plausible precipitation estimates. We also disprove that this influence is *very likely*, as the 90% lower bound on the risk ratio estimate is less than unity (not shown). The Granger interpretation of these statements establishes an upper bound on the uncertainty language ([*Mastrandrea et al.*, 2010]), based on the length of observational record with a fixed number of hurricanes. This conclusion motivates future dynamical climate modeling studies of this event that could arrive at stronger conclusions by enabling the simulation of a large number of factual and counterfactual storms.

In addition to quantifying changes in the probability of the observed Hurricane Harvey precipitation, it is also useful to estimate the amount of excess precipitation attributable to global warming. We do this here by estimating the change since 1950 in return value for the (fixed) contemporary probability estimate of the observed precipitation total. In other words, we estimate the return period, w, for an estimated precipitation total z in 2017 using current values of the Niño3.4 index and CO_2 levels. We then compare the return value z^* at this same return period w estimated with the current Niño3.4 index but 1950 CO_2 levels to the actual observation as a percent change. Best estimates of the attributable percent difference are provided in Table 1 for the range of estimated Hurricane Harvey precipitation, along with the *likely* (66%) lower confidence bound. In the small region, the best estimate of the change is well over 30% for all data sources, with a *likely*

increase around 18-19%. In the large region the best estimate of this attributable difference is lower, around 23%, with a *likely* increase of about 5-7%. These more mechanistic attribution statements ([*Easterling et al.*, 2016]) are to be interpreted as lower bounds on the change in magnitude and upper bounds on the uncertainty language, again as dictated by the Granger causality framework. Previous analysis ([*Pall et al.*, 2017]) suggests that the local warming of the Gulf of Mexico attributable to anthropogenic climate change is about 1°C since the preindustrial era. As most of that warming occurred after 1950, a plausible lower bound on the excess total precipitation during Hurricane Harvey is 6-7% as dictated by the Clausius-Clapeyron (C-C) scaling of saturation specific humidity ([*Allen and Ingram*, 2002]). While our *likely* estimate for the lower bound in the large region is consistent with C-C scaling, it is substantially larger for the wetter small region. A possible interpretation for this result is that within the most heavily precipitating parts of Hurricane Harvey, precipitation efficiency is increased due to factors other than C-C scaling ([*Pall et al.*, 2017]) but at larger scales total precipitation is indeed limited by the amount of available humidity. The consistency of our lower bound on the magnitude of precipitation changes in the large region with C-C scaling enhances confidence in the Granger interpretation of our statistical model's results. Confirmation or dispute of this interpretation again requires dynamical climate modeling studies of this event.

5. Conclusions

Significant changes in both the likelihood and magnitude of observed precipitation totals in the Houston, Texas region from Hurricane Harvey are *likely* attributable to anthropogenic climate change. These conclusions are consistent with a related analysis of

the 2016 flooding in Louisiana ([*van der Wiel et al.*, 2017]), although our attribution statement is more conservative. We interpret our attribution statement in the Granger causality sense, as it is a result of a nonstationary extreme value statistical analysis of the observations alone. As such, this statement should be considered as a lower bound both on the changes in frequency, expressed as the risk ratio, and on the magnitude. A stronger attribution statement that could be interpreted in a Pearl causality sense must await dynamical model analyses with explicit intervention to isolate the anthropogenic influences.

We also find that changes in the *likely* lower bound on the risk ratio are relatively insensitive to observational error in precipitation magnitude from Hurricane Harvey. Furthermore, the attributable changes found in this analysis suggest a sizable human influence on this storm's precipitation. In the wettest part of the storm, it is *likely* that the attributable precipitation increase significantly exceeds that suggested from a simple Clausius-Clapeyron scaling dictated by the attributable increases in Gulf of Mexico surface air temperatures. Confidence in such a super Clausius-Clapeyron effect relies on postulating a plausible physical mechanism to increase the storms efficiency in precipitating available moisture (which is likely limited by the Clausius-Clapeyron relationship). Hopefully, dynamical modeling studies will either confirm or dispute this behavior.

Finally, we reiterate that Hurricane Harvey was an unusual storm largely due to the lengthy period it spent stalled over Texas. Precipitation rates were not particularly unusual for a hurricane of this magnitude (private communication, Dr. Brook Russell, 2017), and the human-induced changes to precipitation metrics that consider less than the seven-

day storm total are smaller than the results presented here. Also, as mentioned in Section 2, the precipitation totals during Hurricane Harvey are significant outliers relative to the previous historical record. As such, this calls into question the appropriateness of any standard extreme value analysis since the 2017 storm total could be the result of a physical processes that did not occur during 1950-2016. This issue has been encountered in other contexts involving observational data, e.g., wave buoy measurements ([*Timmermans et al.*, 2017]). In our case, the out of sample (i.e., *a priori*) estimates of several thousand year return periods for the observed 2017 precipitation (Figure 2c) are probably too large, given that what we are only considering measurements dating back to 1950. Regardless, we note that the changes in extreme statistics of hurricane season precipitation along the Texas coast are remarkably robust. This is evident in the lower bound of the risk ratios in Figure 2(d), which are stable over a large range of storm total precipitation from the previous record of around 300mm to well above the 2017 observations.

Acknowledgments. The authors would like to thank William D. Collins and Benjamin W. Timmermans for helpful discussions, as well as two anonymous reviewers for helpful comments and suggestions. The data supporting this article are based on publicly available measurements from the National Centers for Environmental Information (at `ftp://ftp.ncdc.noaa.gov/pub/data/ghcn/daily/`). We furthermore note that the key points report what is learned from this study.

This research was supported by the Director, Office of Science, Office of Biological and Environmental Research of the U.S. Department of Energy under Contract No. DE-AC02-05CH11231.

References

Allen, M. R., and W. J. Ingram (2002), Constraints on future changes in climate and the hydrologic cycle, *Nature*, *419*(6903), 224.

Coles, S. (2001), *An Introduction to Statistical Modeling of Extreme Values*, Lecture Notes in Control and Information Sciences, Springer.

Compo, G. P., and P. D. Sardeshmukh (2010), Removing ENSO-related variations from the climate record, *Journal of Climate*, *23*(8), 1957–1978.

Cooley, D., D. Nychka, and P. Naveau (2007), Bayesian spatial modeling of extreme precipitation return levels, *Journal of the American Statistical Association*, *102*(479),

824–840, doi:10.1198/016214506000000780.

Easterling, D. R., K. E. Kunkel, M. F. Wehner, and L. Sun (2016), Detection and attribution of climate extremes in the observed record, *Weather and Climate Extremes*, *11*, 17–27.

Ebert-Uphoff, I., and Y. Deng (2012), Causal discovery for climate research using graphical models, *Journal of Climate*, *25*(17), 5648–5665.

Granger, C. W. (1969), Investigating causal relations by econometric models and cross-spectral methods, *Econometrica: Journal of the Econometric Society*, pp. 424–438.

Hannart, A., J. Pearl, F. Otto, P. Naveau, and M. Ghil (2016), Causal counterfactual theory for the attribution of weather and climate-related events, *Bulletin of the American Meteorological Society*, *97*(1), 99–110.

Jeon, S., C. J. Paciorek, and M. F. Wehner (2016), Quantile-based bias correction and uncertainty quantification of extreme event attribution statements, *Weather and Climate Extremes*, *12*, 24–32.

Mastrandrea, M. D., C. B. Field, T. F. Stocker, O. Edenhofer, K. L. Ebi, D. J. Frame, H. Held, E. Kriegler, K. J. Mach, P. R. Matschoss, et al. (2010), Guidance note for lead authors of the IPCC fifth assessment report on consistent treatment of uncertainties.

National Academy of Sciences (2016), *Attribution of Extreme Weather Events in the Context of Climate Change*, The National Academies Press, Washington, DC, doi: 10.17226/21852.

Paciorek, C. (2016), *climextRemes: Tools for Analyzing Climate Extremes*, R package version 0.1.2.

Paciorek, C. J., D. A. Stone, and M. F. Wehner (2017), Quantifying uncertainty in the attribution of human influence on severe weather, *arXiv preprint arXiv:1706.03388*.

Pall, P., M. F. Wehner, and D. A. Stone (2014), Probabilistic extreme event attribution, in *Dynamics and Predictability of Large-Scale, High-Impact Weather and Climate Events*, edited by R. Grojahn, J. Li, R. Swinbank, and H. Volkert, pp. 37–46, Cambridge University Press.

Pall, P., C. M. Patricola, M. F. Wehner, D. A. Stone, C. J. Paciorek, and W. D. Collins (2017), Diagnosing conditional anthropogenic contributions to heavy Colorado rainfall in September 2013, *Weather and Climate Extremes*.

Patricola, C. M., R. Saravanan, and P. Chang (2014), The impact of the El Niño–Southern Oscillation and Atlantic meridional mode on seasonal Atlantic tropical cyclone activity, *Journal of Climate*, *27*(14), 5311–5328.

Pearl, J. (1988), *Probabilistic reasoning in intelligent systems: networks of plausible inference*, 2 ed., Morgan Kaufmann.

Ramaswamy, V., O. Boucher, J. Haigh, D. Hauglustaine, J. Haywood, G. Myhre, T. Nakajima, G. Shi, and S. Solomon (2001), Radiative forcing of climate change, in *Climate Change 2001: The Scientific Basis. Contribution of Working Group I to the Third Assessment Report of the Intergovernmental Panel on Climate Change*, edited by J. T. Houghton, Y. Ding, D. J. Griggs, M. Noguer, P. J. van der Linden, X. Dai, K. Maskell, and C. Johnson, pp. 349–416, Cambridge University Press.

Risser, M. D., D. A. Stone, C. J. Paciorek, M. F. Wehner, and O. Angélil (2017), Quantifying the effect of interannual ocean variability on the attribution of extreme climate

events to human influence, *Climate Dynamics*, doi:10.1007/s00382-016-3492-x.

Timmermans, B., D. Stone, M. Wehner, and H. Krishnan (2017), Impact of tropical cyclones on modeled extreme wind-wave climate, *Geophysical Research Letters*, *44*(3), 1393–1401.

van der Wiel, K., S. B. Kapnick, G. J. van Oldenborgh, K. Whan, S. Philip, G. A. Vecchi, R. K. Singh, J. Arrighi, and H. Cullen (2017), Rapid attribution of the august 2016 flood-inducing extreme precipitation in south louisiana to climate change, *Hydrology and Earth System Sciences*, *21*(2), 897.

Winton, M., K. Takahashi, and I. M. Held (2010), Importance of ocean heat uptake efficacy to transient climate change, *Journal of Climate*, *23*(9), 2333–2344.

Table 1. Precipitation totals (Pr) in mm for the Houston, Texas area over August 25-31, 2017, averaged over each region for each data source. Also shown is the percent change in the magnitude of the observed storm totals from each data source due to human-induced climate change with *likely* lower bound. See Section 4 for more details.

	Small region			Large region		
Data source	(Pr, mm)	Human-induced change in mag. (%)	Lower bound on change (%)	(Pr, mm)	Human-induced change in mag. (%)	Lower bound on change (%)
GHCN stations (raw values)	735.0	37.7	18.8	491.6	23.6	6.8
GHCN stations (smoothed)	700.2	37.7	19.3	481.6	23.6	6.9
NOAA AHPS	829.3	37.7	18.3	552.4	23.7	4.8

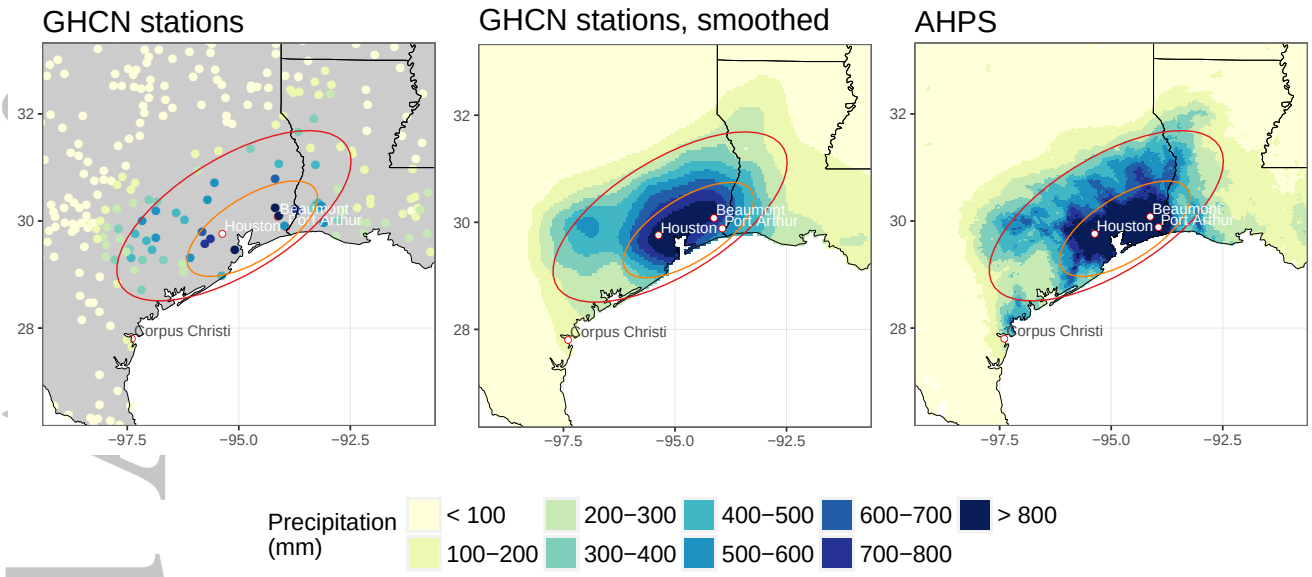

Figure 1. Precipitation totals (mm) for the Houston, Texas region from August 25-31, 2017: GHCN stations with at least 5 non-missing daily measurements during this time window (left); smoothed estimates (using a stationary Gaussian process and kriging) of the GHCN station totals (center); NOAA's Advanced Hydrologic Prediction Service (AHPS) estimates, based on radar and rain gauge data (right). The orange and red ellipses correspond to the small and large regions, respectively.

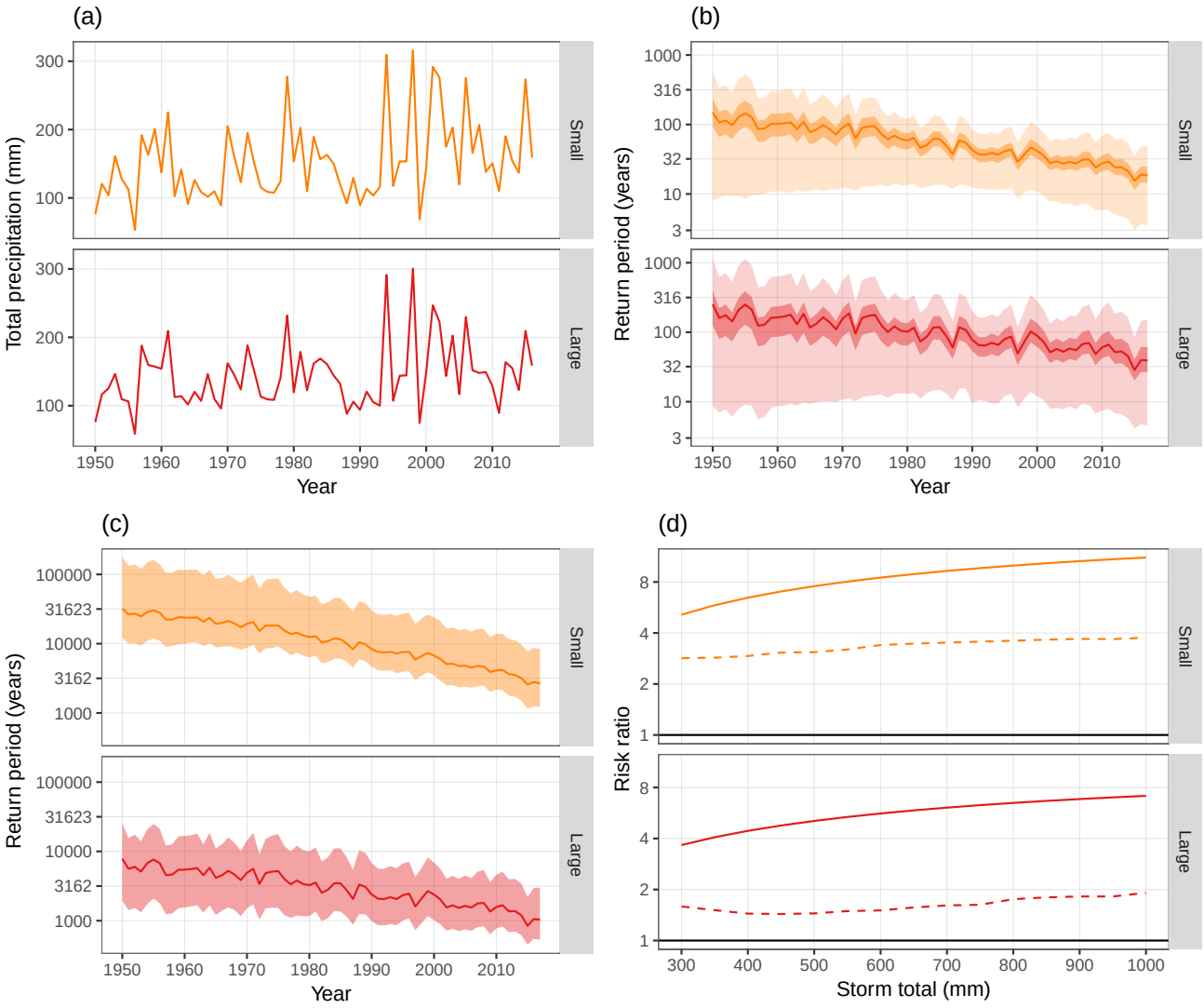

Figure 2. **(a)** Annual values for the largest seven-day total (Rx7day) over 1950-2016, averaged across GHCN stations with non-missing values within each region. **(b)** Return period for the previous largest observed Rx7day (solid line; small region = 315.8 mm, large region = 300.3 mm), with 66% (dark band) and 90% (light band) confidence intervals, using observed Niño3.4 and CO_2 measurements. **(c)** Return period for the observed storm total from Hurricane Harvey (using the raw station average from Table 1) with 66% confidence interval, again using observed Niño3.4 and CO_2 measurements. **(d)** Risk ratio comparing the probability of a range of storm totals z for fixed 2017 Niño3.4 but 2017 CO_2 vs. 1950 CO_2 (solid line) with *likely* lower bound (dashed line).